ELSEVIER

Physica A 247 (1997) 159–182

PHYSICA A

Rods near curved surfaces and in curved boxes

K. Yaman [a], M. Jeng [a], P. Pincus [a], C. Jeppesen [b], C.M. Marques [c,*]

[a] *Department of Physics, University of California, Santa Barbara, CA 93106–9530, USA*

[b] *Materials Research Laboratory, University of California, Santa Barbara, CA 93106, USA*

[c] *R.P.-C.N.R.S., Complex Fluids Laboratory UMR166, Cranbury, NJ 08512–7500, USA*

Received 2 June 1997

Abstract

We consider an ideal gas of infinitely rigid rods near a perfectly repulsive wall, and show that the interfacial tension of a surface with rods on one side is lower when the surface bends towards the rods. Surprisingly we find that rods on both sides of surfaces also lower the energy when the surface bends. We compute the partition functions of rods confined to spherical and cylindrical open shells, and conclude that spherical shells repel rods, whereas cylindrical shells (for thickness of the shell on the order of the rod-length) attract them. The role of flexibility is investigated by considering chains composed of two rigid segments.

PACS: 87.22.Bt; 11.30.Qc; 82.70.Dd

Keywords: Colloids; Depletion; Rod solutions; Membranes

1. Introduction

Macromolecular surface interactions play an important role in a variety of phenomena: stabilization/destabilization of colloidal solutions [1], where the "surface" is the surface of a colloidal particle; surface effects in liquid crystal displays [2], where the "surface" is the walls of the container; and modification of bending rigidities of bilayers [3], in which case the "surface" is a membrane.

Both rigid and flexible macromolecules can induce a modification of the properties of interfaces, either by adsorption or depletion; here we concentrate on the surface physics of non-adsorbing, rigid and rod-shaped macromolecules. Interest in solutions of rigid rod-like objects can be traced to the work of Stanley who first extracted the tobacco mosaic virus (TMV) [4] and to the subsequent observation of the nematic phase in TMV solutions [5], which was later explained by the seminal theory of Onsager [6]. Many other rod-like molecules exist in the biological realm, ranging from DNA in its

* Corresponding author. Fax: +1 609 860-0165; e-mail: marques@phoenix.princeon.edu.

PII S0378-4371(97)00405-6

α-helix form [7] to fibrils of amyloid β-protein, the molecular agent at the origin of the Alzheimer disease [8]. Solutions of rod-like molecules in a large variety of mineral and organic systems have also been studied [9].

In a pioneering study of *surface* interactions of macromolecules Asakura and Oosawa [10] showed that the steric depletion of rigid macromolecules at a flat surface increases the interfacial energy of the system, implying that two surfaces in a solution of non-interacting rods will attract one another when they are at separations smaller than the rod-length. This effect, which is at the origin of colloidal destabilization, is also present in the steric depletion of spherical particles, or particles with other shapes – but with a different range and magnitude. Asakura and Oosawa theory has since been extended to include effects of nematic ordering in the bulk [11,12] or effects of rod–rod excluded volume interactions [13]; in the latter work the authors show that when the modification of the rod–rod excluded volume interactions close to the surface is taken into account, a rod solution may *stabilize* a colloidal suspension, rather than destabilizing it. However, almost all the available studies on rod–surface interactions are devoted to flat geometries, except for Auvray's work [14] where the author makes a first attempt at considering curved geometries; we use some of his constructions in our work, which extends the original Asakura and Oosawa theory to include effects of surface curvature in the contribution of the rod depletion layer to the surface tension. For flexible surfaces, e.g. membranes, in rod solutions, our results allow us to derive the renormalization of the bending rigidities of the membrane. Some of our findings are qualitatively different from the corresponding results for flexible polymers in solution. This prompted us to consider two rigid rod-segments joined in the middle as a first step in studying the cross-over from rigid rods to flexible polymers – rigid rods being a polymer of which the persistence length is longer than its length, and the rod-segments joined in the middle being one with a persistence length equal to half of its length. Not surprisingly we find that when one allows for a hinge in the rod, the results are closer to the flexible polymer results.

Even though steric effects are purely entropic and exist for any non-adsorbing macromolecular solution, the strength of the effects is larger for rods with large aspect ratios. The following simple comparison of the order of magnitudes of the contributions to the surface tension with those caused by spherical particles illustrates this. The typical scale of the energy density in a solution of colloidal spheres of radius r_0 and particle number density ρ_b is $k_BT\rho_b$. Integration over the layer thickness results in corrections to the interfacial energy of the order of $\Delta\gamma \simeq k_BT\rho_b r_0$. On the other hand, the scale for the interfacial tension in most liquids is of the order of $\gamma_0 \simeq k_BT/a^2$ where a is a microscopic size. For instance for $a \sim 0.1$ nm, γ_0 is of the order of tens of mN/m. The depletion of spherical particles, even at order unity volume fractions $\phi = \rho_b(4\pi/3)r_0^3$, induces thus corrections to the interfacial tension which are a factor $(a/r_0)^2$ lower than typical values. Curvature corrections to the interfacial energy are of the form: $\Delta\gamma \simeq k_BT\rho_b r_0(1 + C_1 r_0/R + C_2 r_0^2/R^2)$, where R is the radius of curvature and C_1, C_2 are two numerical constants. This sets the order of magnitude of modifications of the bare elastic constants: $\Delta\kappa \simeq k_BT\rho_b r_0^3$. Even at the upper concentration limit $\rho_b \sim 1/r_0^3$,

these corrections are at the lower end of the range [15], $1-20k_BT$, of most bare elastic constants. For an isotropic rod solution the upper concentration limit is the Onsager concentration $\rho_b^\star = 4.2/(L^2D)$ [6], where L is the length of the rod and D its diameter. Now interfacial tension contributions are of the order $\Delta\gamma \simeq k_BT\rho_bL$, but even for rod diameters of order of the microscopic length a, and at the Onsager concentration this contribution is still a factor (a/L) smaller than typical interfacial tension values. However, modifications of the elastic constants are here of order $\Delta\kappa \simeq k_BT\rho_bL^3$. At the Onsager concentration this is a factor (L/D) larger than k_BT, and therefore, may lead to a substantial modification of the elastic constants of even rather rigid phospholipid membranes with elastic constants as large as $20k_BT$, even at low rod concentrations where rod–rod interactions are negligible.

In the next section we introduce the basic thermodynamics necessary for our discussion; Sections 3, 4 contain our results for rods close to surfaces, and rods in shells, respectively. We make an initial attempt at understanding the cross-over from flexible polymers to rigid rods in Section 5; the last section is devoted to a discussion and summary of our main results.

2. Thermodynamics

We consider an ideal gas of rods of length L in the presence of surfaces which repel the rods, in several different geometries. The thickness of the rods is taken to be zero, i.e. much smaller than all other length scales in the problem. We parametrize the possible rod configurations by the coordinate $\boldsymbol{r}$, and two angles specifying in which direction the rod points, $\boldsymbol{\omega} \equiv \boldsymbol{\omega}(\theta,\phi)$. Kinetics is ignored throughout the treatment [1].

The relevant potential describing the thermodynamics of the system can be written as ($k_BT \equiv 1$)

$$\Omega[\rho(\boldsymbol{r},\boldsymbol{\omega})] = \int d\boldsymbol{r} \int d\boldsymbol{\omega}\, \rho(\boldsymbol{r},\boldsymbol{\omega})[\log(v\,\rho(\boldsymbol{r},\boldsymbol{\omega})/e) - (\mu_b - U_{\text{ext}}(\boldsymbol{r},\boldsymbol{\omega}))]\,, \tag{1}$$

where v is some normalization volume, μ_b is the solution chemical potential, and U_{ext} is the hard wall interaction potential that is either infinite or zero, depending on whether the configuration of the rod is allowed by the "hard wall" requirement or not. Functional minimization of Ω with respect to $\rho(\boldsymbol{r},\boldsymbol{\omega})$ gives the equilibrium density profile:

$$\rho(\boldsymbol{r},\boldsymbol{\omega}) = \frac{e^{\mu}}{v} e^{-U_{\text{ext}}(\boldsymbol{r},\boldsymbol{\omega})} \equiv \frac{\rho_b}{4\pi} e^{-U_{\text{ext}}(\boldsymbol{r},\boldsymbol{\omega})} \tag{2}$$

with ρ_b the rod number density of the bulk solution. The local, position dependent, number density of particles $\rho(\boldsymbol{r})$ is simply the sum over all allowed angular configurations of $\rho(\boldsymbol{r},\boldsymbol{\omega})$. The excess surface energy is then calculated as follows:

$$\Delta\gamma = \frac{\Omega[\rho(\boldsymbol{r},\boldsymbol{\omega})] - \Omega[\rho_b/(4\pi)]}{S} = \rho_b \int \frac{d\boldsymbol{r}}{S} \int \frac{d\boldsymbol{\omega}}{4\pi}(1 - e^{-U_{\text{ext}}(\boldsymbol{r},\boldsymbol{\omega})})\,, \tag{3}$$

[1] Kinetic effects will be smaller by a factor of (thermal wavelength/L) ~ 0.

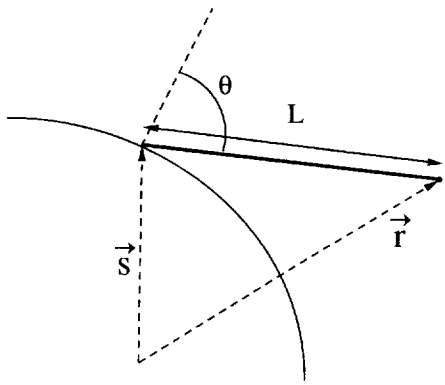

Fig. 1. Configurational space of a rod near a surface. The rod is represented at the angle of contact.

where S is the surface area and the volume integral runs over the space available to the solution.

3. One surface in a rod solution

Here we consider surfaces with rods on one side only. Results for the case with rods on both sides can be easily found by adding the results for the inside and the outside. Our calculations ignore fringe effects that are unimportant in the thermodynamic limit, e.g. the flat wall is treated as translationally invariant.

We first rewrite Eq. (3) in pressure units ($k_B T \rho_b = 1$) and explicitly state its rod-length dependence

$$\Delta\gamma(L) = \int \frac{d\boldsymbol{r}}{S} \int \frac{d\boldsymbol{\omega}}{4\pi} h(\boldsymbol{r}, \boldsymbol{\omega}, L) \,. \tag{4}$$

If we represent the space coordinates of the rod by the position of one extremity (see Fig. 1), the function $h(\boldsymbol{r}, \boldsymbol{\omega}, L)$ is unity when a rod of length L, starting at $\boldsymbol{r}$ and pointing in the direction $\boldsymbol{\omega}$ intersects the surface; it is 0 otherwise. This can be written as $h(\boldsymbol{r}, \boldsymbol{\omega}, L) = H(L - (\boldsymbol{s} - \boldsymbol{r}) \cdot \boldsymbol{\omega})$, with $H(x)$ the usual step function $H(x > 0) = 1$; $H(x < 0) = 0$ and $\boldsymbol{s}$ is defined as follows: The half-ray orginating at $\boldsymbol{r}$ and travelling in the direction of $\boldsymbol{\omega}$ may or may not intersect the surface. If it does not then we do not have to define $\boldsymbol{s}$, since all such configurations give $H = 0$, and thus do not affect any of the below expressions. If the half-ray does intersect the surface, we define $\boldsymbol{s}$ as the intersection point that is closest to $\boldsymbol{r}$. Notice that $\boldsymbol{s}$ is independent of L.

It is convenient to calculate the L-derivative of the excess surface energy:

$$\frac{\partial}{\partial L}\Delta\gamma(L) = \int \frac{d\boldsymbol{r}}{S} \int \frac{d\boldsymbol{\omega}}{4\pi} \delta(L - (\boldsymbol{s} - \boldsymbol{r}) \cdot \boldsymbol{\omega}) = \int \frac{d\boldsymbol{s}}{S} \int \frac{d\boldsymbol{\omega}}{4\pi} \cos\theta_s \, g(\boldsymbol{s}, \boldsymbol{\omega}, L) \tag{5}$$

with θ_s the angle between the rod and the normal to the surface at point s and $g(s,\omega,L)$ a function restraining the angular integration space for a rod with one extremity at s. The integral over ds ranges over the whole surface. The factor $\cos\theta_s$ is the appropriate Jacobian.

3.1. Convex bodies

For any surface delimiting a convex body, the function $g(s,\omega,L)$ restricts the angular integral to half of the angular space, independently of the actual surface shape,

$$\frac{\partial}{\partial L}\Delta\gamma(L) = \frac{1}{4\pi}\int_0^{2\pi} d\phi \int_0^{\pi/2} d\theta \sin\theta\cos\theta = \frac{1}{4}. \tag{6}$$

Integrating Eq. (6) with the boundary condition $\Delta\gamma(L=0)=0$ one gets the three dimensional result for the surface tension of convex bodies immersed in a rod solution:

$$\Delta\gamma(L) = \frac{L}{4}. \tag{7}$$

This result can easily be extended to convex bodies in an arbitrary dimension $\mathscr{D}$:

$$\Delta\gamma(L) = c(\mathscr{D})L \tag{8}$$

with

$$c(\mathscr{D}) = \frac{\Gamma(\mathscr{D}/2)}{2\sqrt{\pi}\,\Gamma((\mathscr{D}+1)/2)} = \frac{(\mathscr{D}-2)!!}{(\mathscr{D}-1)!!} \times \begin{cases} \frac{1}{2} & \text{for } \mathscr{D} \text{ odd}, \\ \frac{1}{\pi} & \text{for } \mathscr{D} \text{ even}. \end{cases} \tag{9}$$

In particular, $c(2) = 1/\pi$ and $c(3) = 1/4$.

3.2. General surfaces

For a general surface, the function $g(s,\omega,L)$ might restrict the angular integration in Eq. (5) to less than half of the angular space. In this case we can still integrate over half of the angular space and further subtract the non-available angular sector. In three dimensions:

$$\frac{\partial}{\partial L}\Delta\gamma(L) = \frac{1}{4} - \int \frac{ds}{S} \int \frac{d\omega}{4\pi} \cos\theta_s H(L - (s'-s).\omega), \tag{10}$$

where s' is another surface vector. Differentiating with respect to L and performing the angular integration leads to

$$\frac{\partial^2}{\partial L^2}\Delta\gamma(L) = -\int \frac{ds}{S} \int \frac{d\ell}{4\pi L^2} \cos\theta_s \cot\theta_\ell. \tag{11}$$

The vector ℓ defines all the points on the surface at a distance L from a given point s. In this three dimensional case this is usually a one dimensional curve. The angle θ_s is

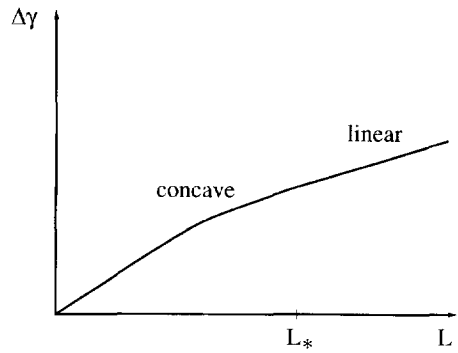

Fig. 2. General shape of the surface tension as a function of the rod-length; L_* is the maximum length of a line that connects any two points on the surface, without intersecting the surface.

measured with respect to the normal of the surface at point s and the angle θ_ℓ is measured with respect to the surface normal at point ℓ. Contrary to the convex case, the excess surface energy of a non-convex body immersed in a rod solution does depend on the actual shape of the body. Moreover, because the contribution of the second order derivative of Eq. (11) is always negative, any long-wavelength concavity will *reduce* the surface tension of a surface with rods on one side or both sides. Therefore entropic effects in such systems will render flat surfaces unstable towards long-wavelength curvature! It also implies that for a *fixed geometry* the surface tension is a concave function of the rod-length, L, and will have the general form depicted in Fig. 2.

Eq. (11) can easily be extended to spaces of different dimensions. For instance, in two dimensions, where the "surface" is actually a one dimensional curve of perimeter P, one has

$$\frac{\partial^2}{\partial L^2}\Delta\gamma(L) = -\int \frac{d\ell}{P} \sum_{q} \frac{1}{2\pi L} \cos\theta_\ell \cot\theta_q \,. \tag{12}$$

The sum runs over all (usually two) points q at a distance L from a given point ℓ on the surface.

3.3. Some examples

With the above methods, $\Delta\gamma(L)$ can be calculated exactly for the inside and outside of a circle, a sphere, and a cylinder, each with radius R; and also for two flat walls separated by δ, i.e. a gap. We would like to emphasize that *all* of these results can also be derived in an independent way which is also exact, namely by "counting beans", i.e. by just doing the integrals in Eq. (4) straightforwardly (see Section 3.5 below). We have explicitly checked that all of the results quoted here agree with these straightforward calculations – especially in the cylinder's case both calculations are quite involved algebraically, and this check is absolutely non-trivial. Of course,

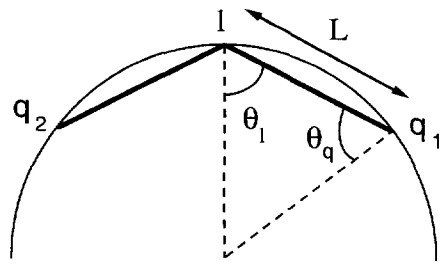

Fig. 3. Rods inside a circle.

the method of computing the second derivative and then integrating up is the shortest route to these answers.

We now define $\varepsilon \equiv L/R$; this is for convenience only and does not mean that we take ε to be small unless specifically stated.

We first calculate results for two dimensions. Inside of a circle we have, (see Fig. 3): $\cos\theta_\ell = \varepsilon/2$, $\cot\theta_q = \cot\theta_\ell = (\varepsilon/2)/\left(\sqrt{1-\varepsilon^2/4}\right)$, and the sum over q amounts to a factor of two. Thus:

$$\frac{\partial^2}{\partial L^2}\Delta\gamma_{\mathrm{cir}}^{\mathrm{in}} = -\frac{1}{\pi L}\cos\theta_\ell \cot\theta_q = -\frac{\pi}{R}\frac{\varepsilon/4}{\sqrt{1-\varepsilon^2/4}}\,. \tag{13}$$

Using $\Delta\gamma(L=0)=0$, and $\dfrac{\partial}{\partial L}\Delta\gamma(L=0) = \dfrac{1}{\pi}$, we find:

$$\frac{\Delta\gamma_{\mathrm{cir}}^{\mathrm{in}}}{L} = \frac{1}{\pi\varepsilon}\sin^{-1}(\varepsilon/2) + \frac{1}{2\pi}\sqrt{1-\varepsilon^2/4}\,. \tag{14}$$

For three dimensions we consider rods inside spheres and cylinders. Inside of a sphere we have, (see Fig. 4): $\cos\theta_s = \varepsilon/2$, $\cot\theta_\ell = \cot\theta_s = (\varepsilon/2)/\left(\sqrt{1-\varepsilon^2/4}\right)$ and $\ell = 2\pi L\sin\theta_s$. Thus:

$$\frac{\partial^2}{\partial L^2}\Delta\gamma_{\mathrm{sph}}^{\mathrm{in}} = -\frac{1}{2L}\sin\theta_s\cos\theta_s\cot\theta_s = -\frac{1}{8}\frac{\varepsilon}{R}\,. \tag{15}$$

It follows that

$$\frac{\Delta\gamma_{\mathrm{sph}}^{\mathrm{in}}}{L} = \frac{1}{4} - \frac{1}{48}\varepsilon^2\,. \tag{16}$$

The calculation for the inside of a cylinder is a bit tedious, but can be done. We find:

$$\frac{\partial^2}{\partial L^2}\Delta\gamma_{\mathrm{cyl}}^{\mathrm{in}} = \frac{8}{3\pi R\varepsilon^3}\left[\left(1+\frac{\varepsilon^2}{4}\right)E\left[\frac{\varepsilon^2}{4}\right] - \left(1+\frac{\varepsilon^2}{8}\right)K\left[\frac{\varepsilon^2}{4}\right]\right], \tag{17}$$

where the functions E and K are the complete elliptic integral of the first and second kind, respectively. The cylinder result can in principle be integrated to give the special functions MeijerG. The straightforward "bean-counting" mentioned above leads also to an integral form that can only be done explicitly as a perturbation series in ε.

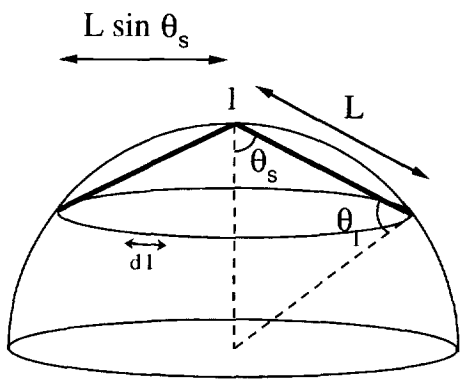

Fig. 4. Rods inside a sphere.

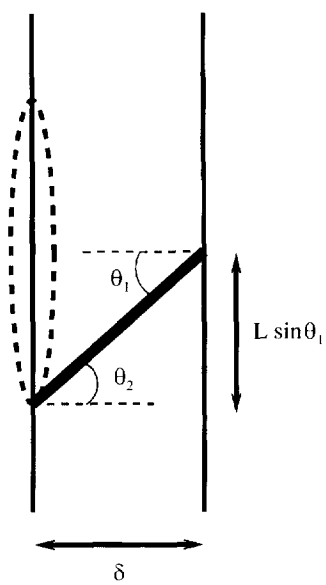

Fig. 5. Rods in a flat gap – side view.

We checked that the coefficients in this series agree with the expression for the second derivative in Eq. (17). The perturbative result for the inside of the cylinder is

$$\frac{\Delta\gamma_{\mathrm{cyl}}^{\mathrm{in}}}{L} = \frac{1}{4} - \frac{1}{128}\varepsilon^2 + \cdots . \tag{18}$$

The case of the flat gap has a different topology, and therefore is worth doing as an example, (see Fig. 5.) For $L \leqslant \delta$, clearly there are no configurations of a rod that bridge two points on the surface, and therefore: $\Delta\gamma_{\mathrm{gap}} = L/2$, (to assure consistency with sections to come we took S to be *one* side's area.) Whereas for $L > \delta$, we have

$\theta_1 = \theta_2 = \theta$, $\cos\theta = \delta/L$, and $\ell = 2\pi L \sin\theta$. Thus

$$\frac{\partial^2}{\partial L^2}\Delta\gamma_{\text{gap}} = -\frac{\cos^2\theta}{L} = -\frac{\delta^2}{L^3}\,. \tag{19}$$

It follows that

$$\frac{\Delta\gamma_{\text{gap}}}{L} = \begin{cases} \delta/L - \delta^2/(2L^2)\,, & L \geqslant \delta\,, \\ 1/2\,, & L \leqslant \delta\,. \end{cases} \tag{20}$$

This is to be compared to Eq. (25) below.

We also developed a method to compute the small L expansion of the surface tension for a general surface in two and three dimensions. We leave this discussion to Appendix A, and just note here that the expansions of the expressions for the circle, sphere, and the cylinder agree with this general method's predictions. In particular, that $\Delta\gamma$ is an odd function of L for sufficiently small L follows from this expansion.

3.4. Random insertion sampling

We also tested the surprising prediction of Eq. (7) in the case of an ellipsoid, the simplest non-trivial case in three dimensions, by performing random insertion sampling. Since the prediction for the surface tension is in the limit of a non-interaction gas of rods, we need only consider the behavior of one rod of length L in our numerical experiment.

The algorithm is as follows. We choose a volume V_0 around the ellipsoid of semi-axis A, B, C that is large enough to encompass the ellipsoid and a shell of thickness $L/2$ around the ellipsoid. We then randomly select M center of mass positions and orientations for the rod of length L. The center of mass must be in V_0 excluding V_e, the volume of the ellipsoid itself. By noting the fraction f of insertions that lead to overlap between the rod and the ellipsoid we can express the surface-tension as

$$\Delta\gamma(L) = f \cdot \frac{V_0 - V_e}{S_e} \tag{21}$$

in units of $k_B T \rho_b$. S_e denotes the surface area of the ellipsoid.

When we choose $M = 10^8$, our numerical experiment confirms the prediction $\Delta\gamma(L)/L = 1/4$ within an error-bar of 0.5×10^{-4} for a wide variety of choices for A, B, C, and L. The error-bar on the fraction f is $\sqrt{\frac{f\cdot(1-f)}{M}}$.

3.5. Comments

Although the method of "bean-counting" is less efficient than the one described above, it is nevertheless useful for gaining more insight into the reasons for the counterintuitive results above. In this method one performs first the angular integration over $\rho(\boldsymbol{r}, \omega)$ to obtain the rod density $\rho(\boldsymbol{r})$. In the particular cases of flat, cylindrical and

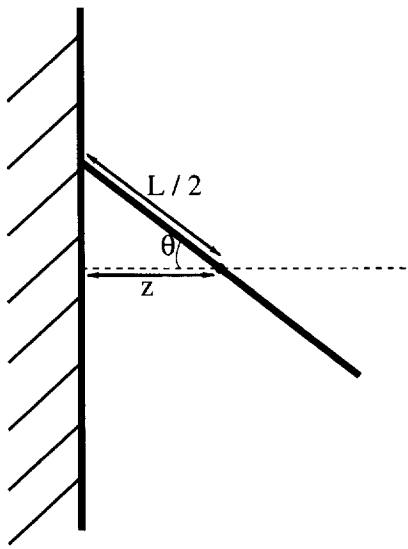

Fig. 6. Configurational space of a rod near a flat surface. The rod is represented at the angle of contact. The complete allowed angular space is obtained by rotation of the figure around the z-axis.

spherical surfaces, the excess surface energy is then obtained from

$$\Delta\gamma = \int dz\,(\rho_b - \rho(z))J(z,R) \tag{22}$$

with z the perpendicular distance from the surface, and $J(z,R)$ the Jacobian, which depends on the geometry. For flat surfaces $J(z,R) = 1$; for the outside of a cylinder of radius R, $J(z,R) = 1 + z/R$, and for a sphere $J(z,R) = (1 + z/R)^2$. For these three geometries there is only a one-dimensional integral (over z) to be carried out, once $\rho(z)$ is determined. Differently from the previous sections, we define hereafter the rod coordinates by the position of its center of mass.

For example, for a plane with rods on one side (see Fig. 6), we have

$$\Delta\gamma_f = \int_0^{L/2} dz \left[1 - \frac{1}{4\pi} \int_0^{2\pi} d\phi \int_{\arccos(2z/L)}^{\pi - \arccos(2z/L)} \sin\theta\, d\theta \right] = \int_0^{L/2} dz \left[1 - \frac{2z}{L} \right] = \frac{L}{4}\,. \tag{23}$$

Notice that the rod concentration $\rho = \rho_b 2z/L$ is different from the monomer concentration. The evaluation of this second quantity is slightly more involved but can be calculated following Auvray [14]. This gives: $c_f(z) = c_b(z/L)(1 - \log(z/L))$, where $c_b = \rho_b N$ is the bulk monomer concentration for a solution of rods with N monomers.

The calculation of the phase space available to a rod in the presence of a curved surface is somewhat different from the one for a flat surface, for now it is possible for the rod to contact the wall in two different ways (see Fig. 7): when the rod is sufficiently

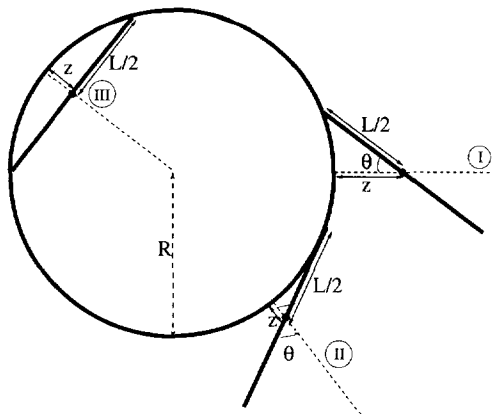

Fig. 7. Configurational space of rods inside and outside a sphere. (I) $z > z_c^{\text{out}}$; (II) $z < z_c^{\text{out}}$; (III) $z = z_c^{\text{in}}$.

far from the surface the tip touches the wall upon rotation, whereas when the rod is sufficiently close to the wall, it will be tangent to the surface at some point along its length. The critical z value separating these two regions is $z_{*,\text{sph}}^{\text{out}} = \sqrt{(L/2)^2 + R^2} - R$. The phase spaces arising from these two configurations have different functional forms. In the inside of the sphere, of course, the tangent construction is not possible, but now there is a minimum distance beyond which it is not possible to place the center of mass of the rod – this happens at $z_{*,\text{sph}}^{\text{in}} = \sqrt{R^2 - (L/2)^2} - R$. A closer look at the results from the previous sections reveals that the surface tension is *non-analytic* in the curvature; e.g. that even for arbitrarily small $\varepsilon = L/R$, one has neither $\Delta\gamma_{\text{sph}}^{\text{out}}(\varepsilon) = \Delta\gamma_{\text{sph}}^{\text{in}}(-\varepsilon)$ nor $\Delta\gamma_{\text{sph}}^{\text{out}}(\varepsilon) = -\Delta\gamma_{\text{sph}}^{\text{in}}(-\varepsilon)$. This invalidates the usual extrapolation of the free energy results from the cylindrical and the spherical shapes to arbitrary bending states. We can see that the difference between $z_{*,\text{sph}}^{\text{out}}$, and $z_{*,\text{sph}}^{\text{in}}$ is the basic reason for this non-analyticity. It is also possible to compute the monomer densities in the spherical configuration, we present these in Appendix B.

From Eq. (23) it is clear that differences between the excess energy of a flat and a curved surface depend on two factors. The first is the configurational part measured by the differences in the rod density profiles, the second one is associated with the space available to the center of mass, and is measured by $J(z,R)$. In the case of hard sphere solutions, where there is no coupling between configuration and curvature, only $J(z,R)$ is responsible for energy differences; the profile of particle concentration, $\rho(z) = \rho_b\,\Theta(z - r_0)$, is independent of geometry. It is easy to show that in that case one has $\Delta\gamma = k_B T\rho_b r_0(1 + r_0/(2R))$ for cylindrical surfaces and $\Delta\gamma = k_B T\rho_b r_0(1 + r_0/R + r_0^2/(3R^2))$ for spherical ones. In the case of rod solutions, there is a coupling between the configuration of the rods and the surface curvature: the concentration profiles are a function of the surface curvature. Given this coupling, the exact correspondence among the free energies of all convex-shaped rod-systems, proven in Section 3.1, is rather surprising. This implies that curvature contributions to free energy Eq. (22), from both the profile and the Jacobian integrate out to a total vanishing value. This cancellation is

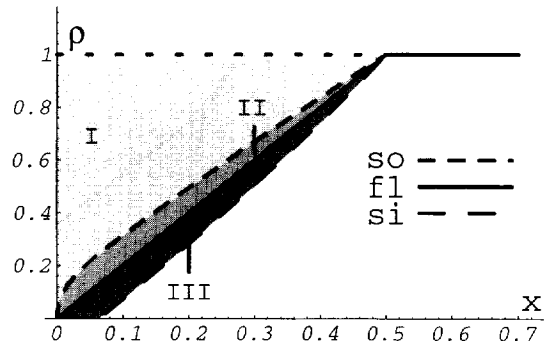

Fig. 8. The rod concentrations, $\rho(x)/\rho_b$, compared for rods inside and outside a sphere and near a flat wall. The distances are in units of L. **so**: Outside of a sphere; **fl**: Flat; **si**: Inside a sphere. We took $R = 2L$ for this picture.

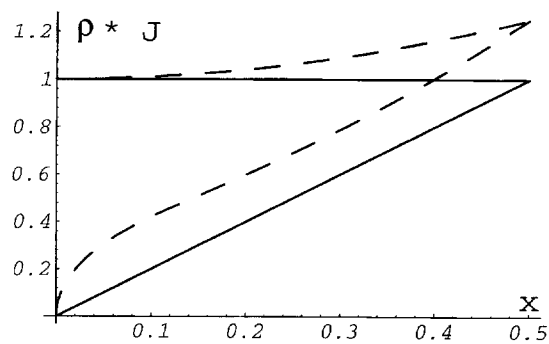

Fig. 9. This plot shows $\rho^{\text{out}}(x)/\rho_b$ weighted by the appropriate Jacobian, for the plane (solid line) and a sphere of radius $R = L$ (dashed line). The result in the text corresponds to the equality of the area between the solid curves to the one between the dashed curves.

non-local, i.e. at a given z away from the surface the total phase space for the center of mass does not change as to compensate for the configurational changes in the profile. One can gain further insight into the issue by recalling Eq. (22), and considering Fig. 8. The surface tension is just the total "area" between the curves $\rho(z)$ and ρ_b *weighted* by the appropriate Jacobian. The surface tension for the plane is simply the sum of the shaded areas I and II, whereas the surface tension for the outside of the sphere is the *weighted* "area" of I only, which happens to be the same. The relevant weighted areas are shown in Fig. 9.

Also, we pointed out that in general the surface tension decreases as the surface develops concave regions, e.g. $\Delta\gamma_{\text{sph}}^{\text{in}} < \Delta\gamma_f$, i.e. the sum of the weighted "areas" of the regions I, II, and III in Fig. 8 is *smaller* than the area of I. Therefore a flat surface with rods on one side would be able to lower its energy by bending *towards* the rods in a spherical shape; and if there are rods on both sides, since $\Delta\gamma_{\text{sph}} < \Delta\gamma_f$, they would destabilize the flat surface towards bending.

3.6. Bending rigidities

For a flexible surface, e.g. a membrane, one computes the renormalization of the bending rigidities by assuming that Δf_c, the excess free energy per unit area of the system is expandable in a power series in the curvature, i.e. the excess free energy is analytic in the curvature. Then up to quadratic order in the principal curvatures $1/R_1$ and $1/R_2$, this expansion can be written in terms of the mean and Gaussian curvatures of the surface [3]. In terms of the principal radii, the mean curvature is $H = 1/2(1/R_1 + 1/R_2)$, and the Gaussian curvature is $K = (1/R_1)(1/R_2)$. A general form of Δf_c to this order is given by: $f_c = 2\Delta\kappa(H - c_0)^2 + \Delta\bar{\kappa}K$, where $\Delta\kappa$ and $\Delta\bar{\kappa}$ are the contributions from the excess free energy to κ and $\bar{\kappa}$, the bare elastic constants of the membrane. c_0 is the induced spontaneous curvature of the system.

As an example we calculate first the modifications of the elastic constants of a membrane immersed in a dilute solution of hard spheres. As quoted above $\Delta\gamma = k_B T\rho_b r_0(1 + r_0/(2R))$ for cylindrical surfaces ($1/R_1 = 1/R$ and $1/R_2 = 0$) and $\Delta\gamma = k_B T\rho_b r_0(1 + r_0/R + r_0^2/(3R^2))$ for spherical surfaces ($1/R_1 = 1/R_2 = 1/R$). This leads to $\Delta\kappa = 0$, $\Delta\bar{\kappa} = (2/3)k_B T\,\rho_b r_0^3$ and $c_0 = 0$.

For a membrane exposed to a rod solution, the non-analyticity of the free energy might imply that the extracted bending rigidities are not meaningful for all states of curvature of the membrane. In particular, bending states where the principal radii of curvature have opposite signs might not be described by the usual Helfrich expansion. With this note of caution in mind, we computed the renormalization of the bending rigidities for a membrane exposed to a rod solution on both sides:

$$c_0 = 0\,, \qquad \Delta\kappa = -\frac{1}{64}\left(\rho_b L^3\right) = \frac{\rho_b}{\rho_b^*}\frac{1}{15.2}\frac{L}{D}\,,$$
$$\Delta\bar{\kappa} = +\frac{1}{96}\left(\rho_b L^3\right) = \frac{\rho_b}{\rho_b^*}\frac{1}{22.9}\frac{L}{D}\,. \tag{24}$$

It is interesting that there is no spontaneous curvature induced by the rods, since there is no symmetry reason why this should be the case. Though, our "small L analysis" in Appendix A shows that this is an (almost) general property of rod-systems. The modifications of the elastic constants (a decrease of κ and an increase of $\bar{\kappa}$ indicating a preference to form periodic minimal surfaces) are similar to results for depletion of other macromolecular species. However, the magnitude of this effect can be here much larger than $k_B T$, a feature not found in other depletion systems. It is of order of $(\rho_b L^3) \simeq (\rho_b/\rho_b^*)(L/D)$, where D is the thickness of the rod and ρ_b^* is the Onsager concentration for rigid rods. Even at the Onsager concentration the enhancement factor L/D can lead to very large contributions.

4. Two surfaces in a rod solution

Here we consider rods in shells where both surfaces of the shells are repulsive. The shells are taken to be in equilibrium with a bulk reservoir of a rod solution at

Table 1
Table of potentials induced by curvature in several systems

System	Spherical	Cylindrical
Quantum particle	Neutral	Attraction
Gaussian chain	Neutral	Attraction
Hard spheres	Repulsion	Neutral
Rods	Repulsion	Attraction

bulk concentration ρ_b. The thickness of the shells is denoted by δ, the perpendicular distance from the inner surface by z. The volume, and the thickness of the box are kept fixed as it gets bent. When $\delta > L$, the results in this section follow from the ones in the previous sections, since the effects of the two surfaces do not interfere with one another. When $\delta < L$ however, there is interference and one needs to calculate the allowed phase space by accounting for interactions with both surfaces.

We consider rods confined inside flat or curved shells, but in equilibrium with a rod solution. By comparing the energies of flat, spherical and cylindrical shells, we hope to investigate for rods a question that has recently been investigated for flexible polymers [16] and mesoscopic quantum systems [17]: do the curved regions in confined systems act as attractive potentials, where the concentration of particles will be greater, or as depletive potentials from where particles will be repelled? Table 1 summarizes the systems studied so far, including the case of confined rods treated below.

4.1. Flat strip

A straightforward calculation for a flat strip of thickness $\delta = yL$ confining a rods solution yields

$$\frac{\Delta\gamma_f^{\text{in}}}{L} = \begin{cases} y - \frac{1}{2}y^2, & y < 1, \\ \frac{1}{2}, & y > 1. \end{cases} \tag{25}$$

As usual, the interfacial energy is expressed in units of $k_B T \rho_b$. Note that for separations larger than the rod-length the interfacial energy is just the sum of two contributions from the inside surfaces. When the surfaces are taken to be also in contact with a solution outside (see Fig. 10) we get

$$\frac{\Delta\gamma_f^{\text{both}}}{L} = \begin{cases} \frac{1}{2} + y - \frac{1}{2}y^2, & y < 1, \\ 1, & y > 1. \end{cases} \tag{26}$$

4.2. Spherical shell

We are able to calculate the available phase space, and thus the surface tension of a spherical shell exactly. The result has four regions, across the boundaries of which

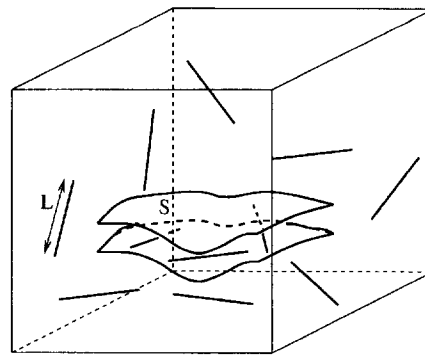

Fig. 10. Rods in a container with an open shell.

the functional form of $\Delta\gamma$ changes. This happens because one needs to consider the relative positions of $z_{*,s}^{\text{out}}$, $z_{*,s}^{\text{in}}$, which were defined earlier, and z_0, the point separating the two regions where the rod only touches the upper surface and the one where it only touches the lower one. The extent of the first two regions vanishes with curvature; the results below tend asymptotically to the ones for the flat strip in the limit of small curvature. We took S as the surface area of the flat box with the same volume and thickness. We leave the full results to the appendix and give here the expansions in $\varepsilon = L/R$,

$$\Delta\gamma_{\text{sph.sh.}}^{\text{in}} = \begin{cases} y\,, & y < \sqrt{\frac{1}{4}+\frac{1}{\varepsilon^2}} - \frac{1}{\varepsilon}\,, \\ y\left(1 - \frac{2\sqrt{2}}{3}\sqrt{y\varepsilon} + \frac{1}{2}\varepsilon + \frac{1}{3\sqrt{2}}(y\varepsilon)^{3/2}\right. & \\ \quad \left. -\varepsilon^2\left(\frac{1}{4}y - \frac{1}{48y}\right) + \mathrm{O}(\varepsilon)^{5/2}\right)\,, & \sqrt{\frac{1}{4}+\frac{1}{\varepsilon^2}} - \frac{1}{\varepsilon} < y < \sqrt{1+\frac{1}{\varepsilon^2}} - \frac{1}{\varepsilon}\,, \\ y - \frac{1}{2}y^2 + \varepsilon^2\left(\frac{1}{24}y^4 + \frac{1}{48}\right) + \mathrm{O}(\varepsilon)^3, & \sqrt{1+\frac{1}{\varepsilon^2}} - \frac{1}{\varepsilon} < y < 1\,, \\ \frac{1}{2} + \varepsilon^2\left(\frac{1}{12}y^2 - \frac{1}{48}\right) + \mathrm{O}(\varepsilon)^3\,, & y > 1\,. \end{cases} \tag{27}$$

One can check by comparing Eq. (25) with Eq. (27) that for any separation the surface tension of the spherical shell is larger than that of the flat box. We conclude therefore that rods prefer to stay in flat regions of the confining box rather than in spherically curved ones. This can be further checked by computing the average rod concentration inside the flat shell and comparing it to the value inside the spherically bent shell; the latter will be smaller than the former. We show below that cylindrical shells induce the opposite, i.e. attract rods, for L less than but close to δ. Results for a spherical shell immersed in a rod solution can be easily obtained by adding to Eq. (27) the outside and inside contributions of Eq. (16).

4.3. Cylindrical shell

The cylindrical shell calculation is substantially more involved than the ones for planar or spherical shells. We resorted to a perturbation in $(1/R)$ in this section, and stayed at separations close to the rod-length, i.e. the results below for $\delta < L$ should be understood to be valid only in a finite region close to L. Again, choosing S as the flat box's surface area, we find

$$\Delta\gamma^{\text{in}}_{\text{cyl.sh.}} = \begin{cases} 1 - \frac{1}{2}y^2 + \frac{1}{128}\left(1 - 4y^2 + 2y^4\right)\varepsilon^2 + \cdots, & y < 1\,, \\ \frac{1}{2} - \frac{1}{128}\varepsilon^2 + \cdots, & y > 1\,. \end{cases} \tag{28}$$

The results for the cylindrical shells are, at least for separations close to the rod-length, opposite of those for the spherical shells: the surface energy in this case is smaller than that for the flat strip. Rod-like molecules will therefore be attracted by cylindrically bent shells.

4.4. Bending rigidities

As explained above, for small curvatures, it is possible to describe the elastic properties of a surface, by three parameters: the spontaneous curvature c_0, and the bending rigidities κ, and $\bar{\kappa}$. In this paragraph we compute these parameters for a flexible box, such as a membrane, exposed to rods. For all cases $c_0 = 0$, as it should be due to the symmetry of the geometry.

For an open shell with rods on the inside only we find

$$\begin{aligned} \Delta\kappa &= -\frac{\rho_b}{\rho_b^*}\frac{L}{D}\begin{cases} \frac{1}{15.2}\left(-1 + 4y^2 - 2y^4\right), & y < 1\,, \\ \frac{1}{15.2}, & y > 1\,, \end{cases} \\ \Delta\bar{\kappa} &= +\frac{\rho_b}{\rho_b^*}\frac{L}{D}\begin{cases} \frac{1}{22.9}\left(-1 + 12y^2 - 2y^4\right), & y < 1\,, \\ \frac{1}{22.9}\left(1 + 8y^2\right), & y > 1\,. \end{cases} \end{aligned} \tag{29}$$

For a strip immersed in a solution of rods, i.e. a system with rods inside and outside the shell we find

$$\begin{aligned} \Delta\kappa &= -\frac{\rho_b}{\rho_b^*}\frac{L}{D}\begin{cases} \frac{1}{15.2}\left(-1 + 4y^2 - 2y^4\right), & y < 1\,, \\ \frac{1}{15.2}, & y > 1\,, \end{cases} \\ \Delta\bar{\kappa} &= +\frac{\rho_b}{\rho_b^*}\frac{L}{D}\begin{cases} \frac{1}{22.9}\left(-1 + 20y^2 - 2y^4\right), & y < 1\,, \\ \frac{1}{22.9}\left(1 + 16y^2\right), & y > 1\,. \end{cases} \end{aligned} \tag{30}$$

5. From rigid rods to flexible polymers

A rigid rod can be viewed as the particular limit of a freely-hinged polymer chain with one monomer only, see Fig. 11. In the reverse limit, when the polymerization

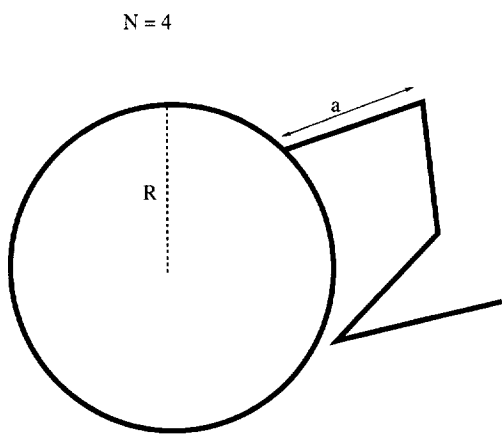

Fig. 11. Segmented rods near surfaces.

number N is very large, the equilibrium configurations of such a chain are well described by Gaussian statistics. We now describe to some extent the crossover between these two limits.

For a membrane in contact with a dilute solution of Gaussian polymers, it is possible to calculate the excess surface energy [18]. For instance, a sphere in $\mathscr{D}$ dimensions immersed in such a solution increases its surface energy by

$$\Delta\gamma_{\text{poly}}(N) = \frac{2}{\sqrt{\pi}} N^{1/2} a + \frac{\mathscr{D}-1}{2}\frac{Na^2}{R} + \frac{(\mathscr{D}-1)(\mathscr{D}-3)}{6\sqrt{\pi}}\frac{N^{3/2}a^3}{R^2} + \cdots \tag{31}$$

with a the monomer size (and total length $L = Na$). For a sphere in three dimensions this reduces to

$$\Delta\gamma_{\text{sph,poly}}(N) = \frac{2}{\sqrt{\pi}} N^{1/2} a + \frac{N a^2}{R} + \cdots . \tag{32}$$

Note that for the Gaussian polymer case, there is an analytical expansion of the free-energy in powers of the curvature, the case of a solution inside a sphere can simply be obtained from the result above by a sign permutation $1/R \to -1/R$. The scaling of the first term in Eq. (32) implies that for a plane the excess surface energy decreases by a factor of $\sqrt{2}$ when one increases by a factor 2 the number of links in a chain of length L.

In the rod limit ($N = 1$), one has in the flat case, $\Delta\gamma_f(N = 1) = (\frac{1}{4})L$. The ($N = 2$)-calculation for the flat case is straightforward and gives

$$\Delta\gamma_f(N = 2) = \frac{5}{24} L , \tag{33}$$

where $L = 2Na$ is still the total length of the polymer. Interestingly, even for such a small monomer number, doubling the number of monomers reduces the surface tension by 1.67, a factor not too different from $\sqrt{2}$ in the Gaussian (large N) limit. It is also

possible to write down a general integral expression for the surface tension near a flat wall for any N where all the integrals are in principle doable; we left this to the appendix, Eq. (C.1).

The surface tension for ($N = 2$) in- and outside of a sphere can be calculated using the same methods as for the rods ($N = 1$). We leave the exact outside result to the appendix, Eq. (C.2), and expand it here in the curvature:

$$\Delta\gamma_{\text{sph}}^{\text{out}}(N = 2) = \frac{5}{24} + \frac{1}{64}\varepsilon - \frac{1}{240}\varepsilon^2 + \cdots. \tag{34}$$

The exact inside result is simply

$$\Delta\gamma_{\text{sph}}^{\text{in}}(N = 2) = \frac{5}{24} - \frac{1}{64}\varepsilon - \frac{13}{1920}\varepsilon^2. \tag{35}$$

Notice that there is now a spontaneous curvature. Moreover, the sign of it is positive for the outside, as it is for ideal polymers [18]. Also, the asymmetry between the in- and the outside cases, which is the cause of the non-analyticity in the curvature free energy, is exactly one-third of what it is for ($N = 1$). Furthermore, the overall magnitude of the ε^2 term is about half of what it is for the rigid rod. This term does not exist for the polymer. Therefore, even the introduction of one single link in the rigid rod, brings the results closer to those of the flexible polymer case.

6. Conclusions

We studied the depletion interactions of curved surfaces exposed to dilute rod solutions. We find that, in general, the excess surface energy caused by the depletion interactions depends on the exact shape of the surface. For instance, the surface tension of a plane exposed to a dilute solution of rods of length L increases by $\Delta\gamma_{\text{flat}} = k_B T\rho_b L/4$, with ρ_b the rod number concentration of the solution, whereas the equivalent quantity for a spherical surface in contact with such a solution *inside* the sphere is $\Delta\gamma_{\text{sph}}^{\text{in}} = k_B T\rho_b L/4 \times (1 - (\frac{1}{12})L^2/R^2)$, with R the radius of curvature of the sphere.

Surprisingly, we found also that a spherical surface in contact with a rod solution *outside* of the sphere has the *same* excess surface energy as the flat surface $\Delta\gamma_{\text{sph}}^{\text{out}} = \frac{1}{4}k_B T\rho_b L$. Moreover we proved that this equality holds for any convex surface exposed to the solution. This implies that the excess energy of any convex body immersed in a dilute rod solution only depends on the total surface of the body and not on its actual shape (as long as it is convex). A similar equality also holds in any dimension of space. For instance in two dimensions, the line tension for a straight line is $\Delta\gamma_{\text{flat}} = k_B T\sigma_b L/\pi$ with σ_b the "bulk" surface rod density, and has the same value for rods outside of a circle.

The first practical implication of our results is that a flexible membrane immersed in a solution (thus exposed to the depletion rod layer on both sides) will spontaneously break its curvature symmetry. Also, a membrane exposed to a rod solution (on one side) will spontaneously bend towards the solution. The experimental observation of

these effects will depend on the magnitude of the symmetry breaking field. This can be measured by comparing the relative importance of induced modifications in the elastic constants of the membrane. Typical values of the bare elastic constants are in the range $1 - 20k_BT$. The induced shift to these bare constants are for most systems like hard spheres or flexible polymers, only a fraction of k_BT. However for rod solutions, at the Onsager concentration, the induced modification is a factor L/D larger than k_BT, and can potentially be very large.

When the rods are confined in curved shells, we showed that regions with cylindrical curvature attract the rods, whereas regions with spherical curvature deplete the rods. This enlightens a recent discussion on confinement effects in solutions of flexible polymers [16] and in mesoscopic quantum systems [17]. Table 1 summarizes results in a variety of systems.

The methods that we developed for this work can be applied to other geometries and other situations. Work is under progress to exactly evaluate rod-mediated sphere–sphere interactions. Also of interest are the effects of attractive interactions on the bending constants of membranes exposed to rod solutions.

We remark also that the steric surface interactions are identical for rigid rods and rigid disks near surfaces, if one takes the rod's length and the disk's diameter to be the same; however the disk system does not enjoy the above-mentioned L/D enhancement. The shell calculations also generalize to the disks if the radius of the disks is sufficiently small.

Acknowledgements

KY and PP acknowledge support from NSF grants DMR-9624091 and MRL-DMR-9632716. CMM was supported by CNRS and NATO fellowships, and by the Petroleum Research Fund (#29306-AC7), administered by the ACS.

Appendix A. Small L expansion

When L is small (or the radii of curvature large) we can expand the excess free energy in powers of L. We do this first for the 2-D case. We start with Eq. (12). For L small, $\sum_q \cos\phi_\ell \cot\phi_q$ is a function only of the point ℓ and the expansion of the shape around it. We assume that L is small enough that rods of length L starting at ℓ can only reach out to points which are nearby along the surface. If the surface is convex in this region, there are no points q, and the function is 0. We ignore inflection points, because they will generally be of measure 0 (except for plane regions, where the function is also 0). We assume that there are no corners. This leaves only regions where the surface is concave. Around the point ℓ we can draw the tangent to the surface as the x-axis, with ℓ at $x = 0$, and let the curve's shape be given by the function $f(x)$ (See Fig. 12). The function f will have a Taylor expansion:

$$f(x) = c_2 x^2 + c_3 x^3 + c_4 x^4 + \cdots , \tag{A.1}$$

where the c_i are functions of ℓ. We want to find the two values of x such that rods of length L start at the origin and hit the curve (see Fig. 12). That is, we need solutions to $x^2 + f(x)^2 = L^2$. There are two solutions, which for L small are near $\pm L$. We can expand in powers of L, and to 4th order find:

$$x_\pm = \pm L \mp \tfrac{1}{2} c_2 L^3 - c_2 c_3 L^4 + \mathrm{O}(L^5)\,. \tag{A.2}$$

It is not hard to show that the two solutions $x_\pm$ are given by the same power series, except with the sign of the odd powers in L reversed. Another way to say this is that the two values of x are given by one power series in $\pm L$. Given the shape $f(x)$ and values $x_\pm$, we can calculate the cosines and cotangents (see Fig. 12)

$$\sum_q \cos\phi_\ell \cot\phi_q = \sum_{x=x_\pm} \frac{f}{L} \frac{xf' - f}{L\sqrt{1+(f')^2}} \Bigg/ \sqrt{1 - \frac{(xf'-f)^2}{L^2(1+(f')^2)}}\,. \tag{A.3}$$

Plugging in the expansion of $x_\pm$ to order L^3 we get

$$\begin{aligned} \cos\phi_\ell \cot\phi_q &= c_2^2 L^2 \pm 3c_3 L^3 + \mathrm{O}(L^4)\,, \\ \sum_q \cos\phi_\ell \cot\phi_q &= 2c_2^2 L^2 + \mathrm{O}(L^4)\,. \end{aligned} \tag{A.4}$$

In the sum over $x_\pm$, the terms of order L^3 canceled out. Because $x_\pm$ is a function of $\pm L$, functions of $x_\pm$ are also functions of $\pm L$. The expression for $\cos\phi_\ell \cot\phi_q$ above uses only functions of $x_\pm$ and $L^2 = (\pm L)^2$, so is again a function of $\pm L$. It follows that when we sum over q, all terms odd in L will cancel out in $\sum_q \cos\phi_\ell \cot\phi_q$, so $d^2\Delta\gamma/dL^2$ and $\Delta\gamma$ are odd functions of L for L small! If we put everything together, and integrate, we get

$$\begin{aligned} \Delta\gamma(L) &= \text{an odd function of } L \\ &= \frac{L}{\pi} - \frac{L^3}{24\pi}\overline{\left(\frac{1}{R^2}\right)} + \mathrm{O}(L^5)\,, \end{aligned} \tag{A.5}$$

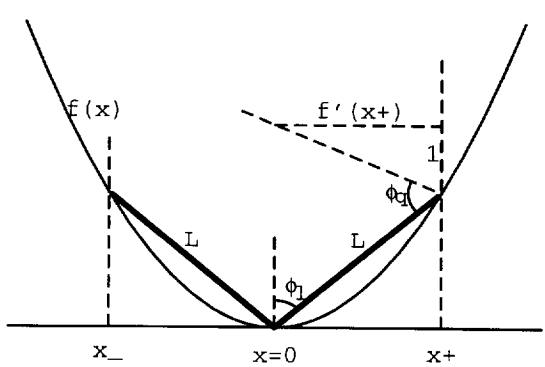

Fig. 12. This construction is used in the computation of the small L expansion of the surface tension.

where R is the local radius of curvature, and $\overline{(1/R^2)}$ indicates that we are averaging $1/R^2$ over the perimeter of the object, weighting by arclength. We set $1/R^2$ to 0 where the object is convex. The assumption that there are no corners is necessary – e.g. for rods inside a rectangle there will be terms of order L^2. And if L is too large, we can no longer do this small L expansion and $\Delta\gamma$ does not have to be an odd function of L – e.g. if we are inside a closed body, and L is larger than all lengths of the body, $\Delta\gamma$ is simply a non-zero constant independent of L.

The expansion in three dimensions is a little more complicated, but essentially the same. We again assume that there are no corners, and that inflection points outside of plane regions are a set of measure 0. We have a tangent xy-plane and a function $f(x, y)$. We expand $f(x, y)$ in powers of x and y, starting at x^2 and y^2 and rotating out the xy term. The solutions to $x^2 + y^2 + f(x, y)^2 = L^2$ are a near-circle. Letting ϕ be the angle in the xy plane, and putting $u^2 \equiv x^2 + y^2$ we have

$$\begin{aligned} f(u,\phi) &= c_{2,\phi}u^2 + c_{3,\phi}u^3 + c_{4,\phi}u^4 + \cdots, \\ c_{2,\phi} &\equiv c_{20}\cos^2\phi + c_{22}\sin^2\phi, \\ c_{3,\phi} &\equiv c_{30}\cos^3\phi + c_{31}\cos^2\phi\sin\phi + c_{32}\cos\phi\sin^2\phi + c_{33}\sin^3\phi. \end{aligned} \tag{A.6}$$

Note that $c_{n,\phi} = (-)^n c_{n,\phi+\pi}$. We now need to look for solutions of $u^2 + f(u,\phi)^2 = L^2$ for each particular ϕ. But this is just the 2-D problem, which has already been done. The only additional complication is the arclength factor, which can be rewritten in spherical coordinates as

$$\begin{aligned} d\ell &= \sqrt{(Ld\theta)^2 + (L\sin\theta\, d\phi)^2} \\ &= d\phi L\sqrt{1 - \cos^2\theta + \tfrac{1}{\sin^2\theta}\left(\tfrac{d(\cos\theta)}{d\phi}\right)^2} \\ &= d\phi L\sqrt{1 - \left(\tfrac{f}{L}\right)^2 + \frac{1}{1-\left(\tfrac{f}{L}\right)^2}\left(\tfrac{d}{d\phi}\left(\tfrac{f}{L}\right)\right)^2}. \end{aligned} \tag{A.7}$$

The values of f at angles ϕ and $\phi + \pi$ have the same power series in $\pm L$, and L only appears independently in $L^2 = (\pm L)^2$. So as in the 2-D case, $\Delta\gamma$ is an odd function of L for L small. The low order expansion in L gives

$$\begin{aligned} \int d\ell\cos\theta_1\cot\theta_2 &= L\int_0^{2\pi} d\phi\,[c_{2\phi}^2L^2 + c_{3\phi}L^3 + \mathrm{O}(L^4)] \\ &= L^3\frac{\pi}{4}(3c_{20}^2 + 2c_{20}c_{22} + 3c_{22}^2) + \mathrm{O}(L^5). \end{aligned} \tag{A.8}$$

Integrating twice and rewriting in terms of the principal radii of curvature,

$$\Delta\gamma(L) = \frac{L}{4} - \frac{L^3}{384}\overline{\left(\frac{3}{R_1^2} + \frac{2}{R_1R_2} + \frac{3}{R_2^2}\right)} + \mathrm{O}(L^5). \tag{A.9}$$

Once again, when taking this average it is understood that we take the quantity inside the parentheses to be zero if the surface is concave at the point at hand. Now in terms of the Gaussian and the mean curvatures:

$$\Delta\gamma(L) = \text{an odd function of } L$$
$$= \frac{L}{4} - \overline{\left(\frac{H^2}{32} - \frac{K}{96}\right)} L^3 + \mathrm{O}(L^5)\,. \tag{A.10}$$

Appendix B. Sphere and spherical shell

The probability of finding a rod's center of mass z away from a sphere can be calculated by first computing the allowed angular phase in Fig. 7 and then integrating over the angles. For convenience we define $r \equiv R/L = 1/\varepsilon$, and still use $x \equiv z/L$. We find for these probabilities

$$\rho^{\mathrm{out}}_{\mathrm{sph}}(x)/\rho_b = \begin{cases} \sqrt{2rx + x^2}/(r + x)\,, & 0 < x < x^{\mathrm{out}}_{*,\mathrm{sph}}\,, \\ 2x + (1/4 - x^2)/(r + x)\,, & x^{\mathrm{out}}_{*,\mathrm{sph}} < x < \frac{1}{2}\,, \end{cases}$$
$$\rho^{\mathrm{in}}_{\mathrm{sph}}(x)/\rho_b = \begin{cases} 0\,, & 0 < x < x^{\mathrm{in}}_{*,\mathrm{sph}} \\ 2x - (1/4 - x^2)/(r - x)\,, & x^{\mathrm{in}}_{*,\mathrm{sph}} < x < \frac{1}{2}\,. \end{cases} \tag{B.1}$$

The monomer concentration inside and outside of a sphere can be computed following the construction in Ref. [14].We define $\lambda_*(r,x) \equiv \frac{1}{2} - \sqrt{(r-x)^2 - r^2 + \left(\frac{1}{2}\right)^2}$:

For the inside of the sphere the concentration profile is given by[2]

$$c^{\mathrm{in}}_{\mathrm{sph}}(x) = \begin{cases} c^{\mathrm{in}}_{\mathrm{sph,I}}(x)\,, & 0 < x < r - \sqrt{(1/2)^2 + r^2}\,, \\ c^{\mathrm{in}}_{\mathrm{sph,II}}(x)\,, & r - \sqrt{(1/2)^2 + r^2} < x < 1\,, \\ c_b\,, & x > 1\,, \end{cases} \tag{B.2}$$

where

$$c^{\mathrm{in}}_{\mathrm{sph,I}}(x) \equiv c_b \left[x - x\log(x) - \frac{1}{2(r-x)} \left(\frac{1}{2}(1 - x^2) + x^2 \log(x) \right) + x \log\left(\frac{\lambda_*}{1 - \lambda_*} \right) \right.$$
$$\left. - \frac{1}{2(r-x)} \left(\frac{1}{2}(\lambda_*^2 - (1 - \lambda_*)^2) - x^2 \log\left(\frac{\lambda_*}{1 - \lambda_*} \right) \right) \right],$$
$$c^{\mathrm{in}}_{\mathrm{sph,II}}(x) \equiv c_b \left[x - x\log(x) - \frac{1}{2(r-x)} \left(\frac{1}{2}(1 - x^2) + x^2 \log(x) \right) \right]. \tag{B.3}$$

[2] Strictly speaking this calculation assumes $L \leqslant R$.

The monomer concentration on the outside of a sphere is[3]

$$c_{\mathrm{sph}}^{\mathrm{out}}(x) = \begin{cases} c_{\mathrm{sph,I}}^{\mathrm{out}}(x), & 0 < x < \sqrt{1+r^2} - r, \\ c_{\mathrm{sph,II}}^{\mathrm{out}}(x), & \sqrt{1+r^2} - r < x < 1, \\ c_b, & x > 1, \end{cases} \tag{B.4}$$

where

$$c_{\mathrm{sph,I}}^{\mathrm{out}}(x) \equiv c_b \left(\frac{1}{4(r+x)}\right)\left(-2rx + 4\sqrt{x(2r+x)} - (2rx+x^2)\log\left(1+\frac{2r}{x}\right)\right),$$

$$c_{\mathrm{sph,II}}^{\mathrm{out}}(x) \equiv c_b \left(\frac{1}{4(r+x)}\right)\left(1 + 4rx + 3x^2 - 2(2rx+x^2)\log(x)\right). \tag{B.5}$$

Notice that the first regimes in both cases disappear as the radius becomes large, and one can readily check that the second regime's profile goes to the flat case's profile in this limit. This concentration profile calculation, for the outside is done in Ref. [14] as well, where the author also finds these three regimes. Our result agrees with his in regimes II and (trivially) III. But we differ in regime I. Since his result is not continuous across the boundary between I and II we believe that his calculation for that case is inaccurate. Our result is continuous, and furthermore the full profile integrates to the full partition function for this geometry, which is a non-trivial consistency check. The profile for the inside is also continuous and integrates to the partition function for the inside of the sphere – again a non-trivial consistency check.

The full, exact expression for the surface tension in a spherical shell is given by

$$\Delta\gamma_{\mathrm{sph}}^{\mathrm{in}} = y\left(1 - \frac{\tilde{v}(y,\varepsilon)}{v(y,\varepsilon)}\right), \tag{B.6}$$

where $v(y,\varepsilon) \equiv y + \varepsilon y^2 + \frac{1}{3}\varepsilon^2 y^3$, and

$$\tilde{v}(y,\varepsilon) = \begin{cases} 0, & y < \sqrt{\frac{1}{4}+\frac{1}{\varepsilon^2}} - \frac{1}{\varepsilon}, \\ \frac{1}{16}\left(8\varepsilon y - 4\varepsilon\sqrt{\varepsilon y(2+\varepsilon y)} + 4\varepsilon^2 y^2 + \varepsilon^2\right) & \\ \quad + \frac{1}{24}\left(8\varepsilon y - 4\varepsilon\sqrt{\varepsilon y(2+\varepsilon y)} + 4\varepsilon^2 y^2 + \varepsilon^2\right)^{3/2}, & \sqrt{\frac{1}{4}+\frac{1}{\varepsilon^2}} < y + \frac{1}{\varepsilon} < \sqrt{1+\frac{1}{\varepsilon^2}}, \\ \frac{1}{2}y^2 + \frac{1}{8}\varepsilon^2 y^4 - \frac{1}{48}\varepsilon^2 + \frac{1}{2}\varepsilon y^3, & \sqrt{1+\frac{1}{\varepsilon^2}} - \frac{1}{\varepsilon} < y < 1, \\ y - \frac{1}{2} + \varepsilon y^2 - \frac{1}{2}\varepsilon y + \frac{1}{3}\varepsilon^2 y^3 - \frac{1}{4}\varepsilon^2 y^2 + \frac{1}{48}\varepsilon^2, & y > 1. \end{cases} \tag{B.7}$$

[3] Strictly speaking this calculation assumes $L \leqslant \frac{4}{3}R$.

Appendix C. Segmented rod results

The integral expression for the surface tension of an N-polymer around a flat surface is

$$\Delta\gamma_f = N - (1/2)^N \int_0^N dz_1 \prod_{i=1}^{N} \left(\int_{-1}^{1} du_i \left[\Theta(z_i - 1) + \Theta(1 - z_i)\,\Theta(z_i - u_i) \right] \right), \tag{C.1}$$

where $z_i \equiv z_1 - \sum_{j=1}^{i-1} u_j$, and Θ is the step-function. This formula gives the same answers as our intuitive way of doing these integrals for ($N = 1$ and 2). With sufficient patience or efficient programming it should be straightforward to see how the result changes as N grows larger.

The exact expression for the surface tension for $N = 2$ outside of a sphere is

$$\Delta\gamma_{\text{sph}}^{\text{out}} = \frac{2}{15}\left(\frac{1}{\varepsilon}\right)^3 \left[\left(1 + \frac{1}{4}\varepsilon^2\right)^{5/2} - \left(1 + \frac{5}{8}\varepsilon^2 - \frac{25}{16}\varepsilon^3 + \frac{1}{32}\varepsilon^5\right) \right]. \tag{C.2}$$

References

[1] W.B. Russel, D.A. Saville, W. Schowalter, Colloidal Dispersions, Cambridge University Press, Cambridge, New York, 1989.
[2] P.G. deGennes, J. Prost, The Physics of Liquid Crystals, Oxford University Press, Oxford, England, 1993.
[3] S. Safran, Statistical Thermodynamics of Surfaces, Interfaces and Membranes, Addison-Wesley, Reading, MA, 1994.
[4] W.M. Stanley, Science 81 (1935) 644.
[5] F.C. Bawden, N.W. Pirie, J.D. Bernal, I. Fankuchen, Nature 138 (1936) 1051.
[6] L. Onsager, Ann. N.Y. Acad. Sci. 51 (1949) 627.
[7] F. Livolant, A. Leforestier, Prog. Pol. Sci. 21 (1996) 1115.
[8] A. Lomakin et al., Proc. Natl. Acad. Sci. USA 93 (1996) 1125.
[9] P.A. Buining, J. Phys. Chem. 97 (1993), 11510 and references therein.
[10] S. Asakura, F. Oosawa, J. Chem. Phys. 22 (1954) 1255.
[11] A. Poniewierski, R. Holyst, Phys. Rev. A 38 (1988) 3721.
[12] B.G. Moore, W.E. McMullen, J. Phys. Chem. 96 (1992) 3374.
[13] Y.A. Mao, M.E. Cates, H.N.W. Lekkerkerker, Phys. Rev. Lett. 24 (1995) 4548.
[14] L. Auvray, J. Phys. (Paris) 42 (1981) 79.
[15] D. Nelson, T. Piran, S. Weinberg (Eds.), World Scientific, London, 1989.Statistical Mechanics of Membranes and Surfaces,
[16] K. Yaman, P. Pincus, F. Solis, T.A. Witten, Macromolecules 30 (1997) 1173.
[17] H. Jensen, H. Koppe, Ann. Phys. 63 (1971) 586.
[18] E. Eisenriegler, A. Hanke, S. Dietrich, Phys. Rev. E 54 (1996) 1134.